Available online at www.sciencedirect.com

SciVerse ScienceDirect

Journal of the European Ceramic Society 32 (2012) 457–463

www.elsevier.com/locate/jeurceramsoc

Effect of pressure on electric generation of PZT(30/70) and PZT(52/48) ceramics near phase transition pressure

Kyung Ho Cho, Chang Eui Seo *, Yoon Soo Choi, Young Ho Ko, Kwang Joo Kim

The 4th R&D Institute-2, Agency for Defense Development, P.O. Box 35-42, Yuseong, Daejeon, 305-600, Republic of Korea

Received 4 June 2011; received in revised form 24 August 2011; accepted 25 August 2011
Available online 21 September 2011

Abstract

Impact experiment of $Pb(Zr_{0.3}Ti_{0.7})O_3$ and $Pb(Zr_{0.52}Ti_{0.48})O_3$ ceramics were conducted by empolying shock reverberation techniques within 3–7 GPa and X-ray diffraction patterns of these materials have been measured at pressure up to 32 GPa with a diamond anvil cell and synchrotron radiation. To refine the crystal structure, Rietveld analysis was performed and bulk moduli were calculated using Birch-Murnaghan equation of state. We found a tetragonal phase transforming to a cubic phase in $Pb(Zr_{0.3}Ti_{0.7})O_3$ and $Pb(Zr_{0.52}Ti_{0.48})O_3$ ceramics at ~7.4 GPa and ~4 GPa respectively. For dynamic pressure experiment, a metal flyer accelerated by a gas gun facility impacts into PZT ceramics to investigate electric energy. As pressure increased, output voltage of $Pb(Zr_{0.3}Ti_{0.7})O_3$ and $Pb(Zr_{0.52}Ti_{0.48})O_3$ ceramics slightly increased below ~7 GPa and ~4 GPa. But the voltage increased near ~7 GPa and ~4 GPa. From the result, we could confirm that the phase transition influenced the considerable effect on the electrical power generation.

Keywords: PZT; Phase transition; Ferroelectric properties; X-ray methods; Electric properties

1. Introduction

PZT ceramics are ferroelectric materials that have found wide application in recent years because of their superior piezoelectric properties.[1–6] Especially, the concern about the moment power device using PZT ceramics increases in the industrial or the military field.[7,8] PZT ceramics were identified many years ago as reversible generator of electrical energy in the fields of acoustics and ultrasonics; however, relatively few studies have been performed to characterize their electrical properties as a ferroelectric power generator under shock wave and structural properties of these materials under high pressure is still limited. It is well established that electrical energy can be obtained from poled ferroelectric ceramics either through their piezoelectric properties or through depoling by shock stress. In the latter case, piezoelectric charge generation is usually of secondary importance compared with the release of the surface charge that compensates the polarization.[9] Depending on the composition of the material, the mechanism of depoling may be either domain switching or a stress-induced phase transition.

The behavior of various PZT ceramics under shock loading shows that obtaining high energy densities ($P^2_r/2\varepsilon$), where P_r is the remanent polarization and ε is the effective permittivity when the bound charge released, requires ceramics having a high remanent polarization and a low permittivity, which release their energy suddenly during shock compression through ferroelectric domain switching or a ferroelectric → paraelectric (nonferroelectric) phase transition.

Although its behavior as a function of temperature at atmospheric pressure has been well studied in terms of structural and dielectric properties, relatively few studies have been performed to know the structural properties of this material under high pressure. Recently we have carried out an angle-dispersive X-ray diffraction study on polycrystalline $Pb(Zr_{1-x}Ti_x)O_3$, where $x = 0.1$, 0.3, 0.4, 0.5, 0.6, 0.7, 0.8, and 0.9 at pressure up to 35 GPa,[10,11] in order to know the pressure dependence of various PZT ceramics, i.e. to know both the pressure and the crystal structure of PZT ceramics where the pressure-induced phase transition occurs.

In this study, X-ray powder diffraction patterns of $Pb(Zr_{0.3}Ti_{0.7})O_3$ and $Pb(Zr_{0.52}Ti_{0.48})O_3$ have been measured

* Corresponding author. Tel.: +82 42 821 2755, fax: +82 42 823 3400.
E-mail address: mylight@kaist.ac.kr (C.E. Seo).

0955-2219/$ – see front matter © 2011 Elsevier Ltd. All rights reserved.
doi:10.1016/j.jeurceramsoc.2011.08.034

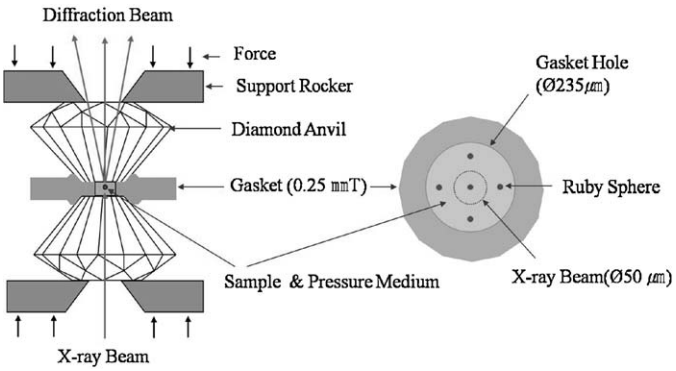

Fig. 1. Schematic diagram of the high-pressure X-ray diffraction experimental set-up.

at pressures up to 32 GPa to know both the pressure and the crystal structure of PZT ceramics where the pressure-induced phase transition occurs. To examine the effect of pressure on the output voltage in $Pb(Zr_{0.3}Ti_{0.7})O_3$ and $Pb(Zr_{0.52}Ti_{0.48})O_3$ ceramics under shock compression near the pressure where phase transition occurs, impact experiments of these materials were conducted by employing shock reverberation techniques within the pressure range of 3–7 GPa in referring to X-ray experimental results.

2. Experimental procedure

2.1. High-pressure X-ray diffraction experiment

In our experiments two kinds of PZT-ceramic samples were prepared with different Zr/Ti ratios [$Pb(Zr_{0.3}Ti_{0.7})O_3$ and $Pb(Zr_{0.52}Ti_{0.48})O_3$, designated as PZT(30/70) and PZT(52/48)]. The polycrystalline samples were prepared by using standard solid state reaction method. The starting powders of ZrO_2, TiO_2 and PbO were finely ground and then calcined at 900 °C for 3 h. After being formed with the isostatic pressing method under 50,000 psi (~345 MPa) pressure that improves the density of samples, and then sintered at 1200 °C for 3 h. Their sintered density were about 7.7 g/cm^3. For the high-pressure X-ray powder diffraction study, the sintered PZT(30/70) and PZT(52/48) samples were repowdered, contained in a spring steel gasket hole of 235 μm diameter, which was drilled by an electric discharge machine (Hylozic Products, Washington, USA), mounted between the two opposed 350 μm diamond culets (D'Anvils Ltd, Hod-Hasharon, Israel) of the Mao-Bell-type diamond anvil cell (Fig. 1).

The pressure medium was a 4:1 methanol–ethanol mixture, which could generate hydrostatic state by the Pascal's law up to 10 GPa.[12] So one have to measure the pressure distribution of a gasket chamber at several points like Fig. 1 to consider the pressure gradient of the gasket chamber more than 10 GPa. A few ruby spheres (RSA Le Rubis SA, Grenoble, France) were included to measure the pressure by the ruby fluorescence method[13–15] with a spectrometer with a Jobin Yvon Triax 320 CCD detector (HORIBA Jobin Yvon S.A.S., Longjumeau Cedex, France) and the R_1 and R_2 fluorescence bands were resolved in all high pressure spectra. An angle-dispersive X-ray powder diffraction experiment was carried out using synchrotron radiation on 5A HFMS wiggler beamline at Pohang Light Source (Fig. 2).

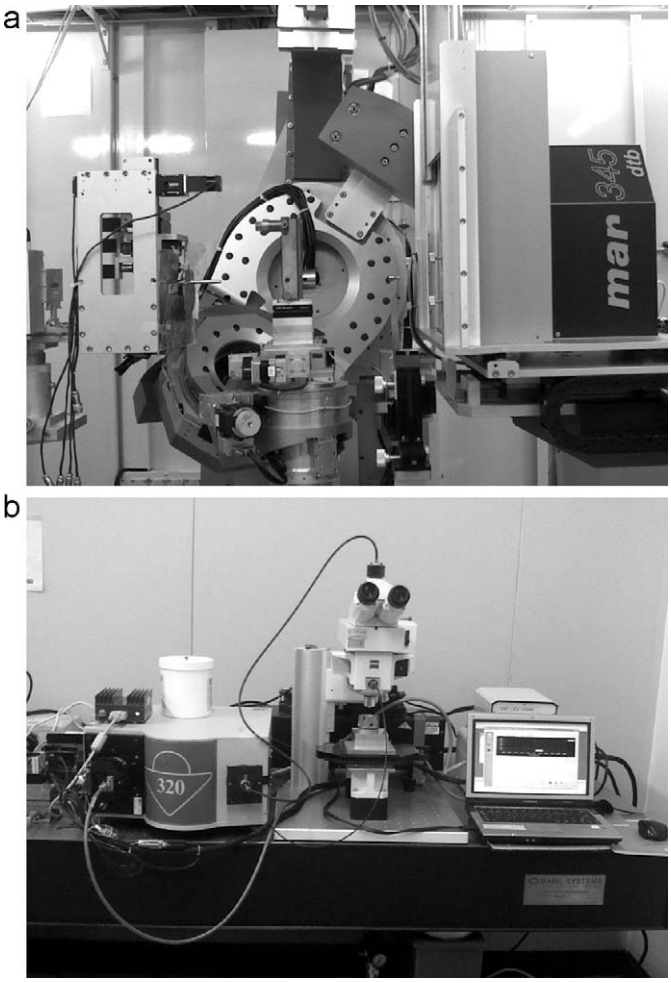

Fig. 2. (a) The high-pressure experiment using a diamond anvil cell on the 5A HFMS wiggler beam line at Pohang Light Source. (b) The spectrometer system for measuring the pressure distribution inside the gasket chamber of a diamond anvil cell.

An incident X-ray beam was monochromatized to the wavelength of 0.61992 Å and collimated to 50 μm diameter using a double pinhole collimator. All diffraction data were collected with a Mar 345 image plate detector (Marresearch GmbH, Norderstedt, Germany) at room temperature, to which the distance (~300 mm) was calibrated using a LaB_6 standard placed at the sample position. The X-ray patterns were collected with an exposure time of 5 min. The integrated 2θ–I patterns were obtained after correction for detector distortion and tilt using the Fit2D package.[16] The computer program TOPAS[17] was used not only to perform Rietveld analysis at 0 GPa for both PZT(30/70) and PZT(52/48) ceramics to refine the ambient-pressure structures[18] but also to refine the lattice parameter and unit-cell volume at high pressures for PZT(30/70) and PZT(52/48) ceramics.

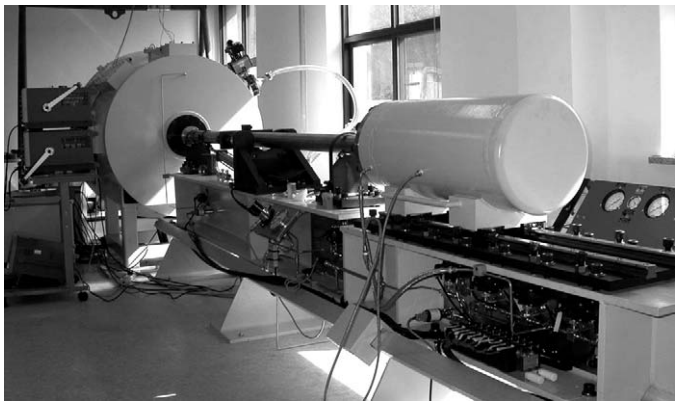

Fig. 3. 40-mm gas gun used for the impact-loading experiment.

2.2. Dynamic impact experiment

For dynamic impact experiment, each sample was fabricated to have the size of 21 mm (L) × 21 mm (W) × 5 mm (T) and was polished. Copper block electrodes having the size of 17 mm (L) × 7 mm (W) × 3 mm (T) were attached to both surfaces of the sample with silver epoxy and electrode terminals were soldered on the other sides of electrodes. Since the impact generates high voltage, the PZT ceramic connected in the electrode and cables was molded with an insulating epoxy resin (EPO-THIN) to avoid electric breakdown inside the sample.

Fig. 3 shows the schematic of the 40-mm gas gun used for the experiment. It consists of a target assembly containing the PZT ceramic that connected by a cable to a high voltage box containing the pulse diagnostics. The experiments were conducted by 40-mm-bore gas gun in which a flyer plate was accelerated to a velocity from 0.1 km/s to 0.5 km/s by using compressed nitrogen at a pressure <1800 psi (~12.4 MPa). Impact tilt is typically less than 3 mrad. Electrical snip-off pins were placed at the final 10 cm inside the barrel to measure the impact velocity. The materials of the flyer and sabot are Al or 304 stainless steel and Acryl. While the chamber is maintained in vacuum less than 0.5 Torr (~66.7 Pa), the flyer accelerated in the barrel impacts the PZT ceramic placed inside the chamber. The impact of the flyer depoles the PZT ceramic, thereby releasing the bound surface charge on the electrodes of the sample. The magnitude of the charge release is controlled by the amount of the bound charge and shock stress in the sample, which depends on the impact velocity. Fig. 4 is a schematic of the experimental arrangement for measuring the output. It consists of a flyer accelerated by the gas gun, a target assembly containing the PZT ceramic, a detector circuit, and an oscilloscope.

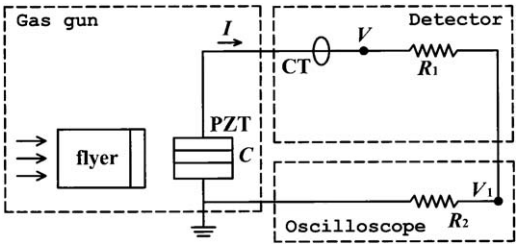

Fig. 4. Schematic of the experimental arrangement for measuring the dynamic impact output.

The electrical response of a shock-compressed ferroelectric ceramic is a complicated phenomenon. We simply analyze the circuit with the assumption that the charges are produced on the surface of the PZT ceramic by a steady shock wave and flow to a load resistor as shown in Fig. 4. As the shock wave passes through the PZT ceramic, the remanent polarization vector P_0 is reduced in magnitude behind the shock front. A simplified model for the release of charge was suggested by Mock et al.[19] under the assumption that the permittivity of the PZT ceramic is constant before and after the shock front. According to the simple model, the charge release $Q(t)$ is represented as follows,

$$\begin{aligned} Q(t) &= P_0 A \frac{t}{\tau}\left(1 - \frac{\alpha t}{P_0}\right), \quad 0 \le t \le \tau, \\ &= P_0 A \left(1 - \frac{\alpha \tau}{P_0}\right), \quad t \ge \tau, \end{aligned} \tag{1}$$

where A is the area of the PZT ceramic surface, τ is the transit time of the shock wave through the PZT ceramic or the length of PZT ceramic divided by the shock velocity, and α represents the linear decrease of the total charge release whose typical value is $0.2P_0/\tau$.[19] The resistance R_2 was ignored because it was much smaller than R_1:

$$R_1 >> R_2. \tag{2}$$

We consider the case that R_1 is not so large so that I_R cannot be ignored. In this case, part of the released charge, as much as

$$I_R = \frac{V(t)}{R_1}, \tag{3}$$

flows through the load resistor. Then the amount of the charge remaining at capacitor C becomes the generated charge represented by Eq. (1) minus the charge that flows through the load resistor, or

$$\begin{aligned} Q(t) &= P_0 A \frac{t}{\tau}\left(1 - \frac{\alpha t}{P_0}\right) - \int_0^t dt_1 \frac{V(t_1)}{R_1}, \quad 0 \le t \le \tau, \\ &= P_0 A \left(1 - \frac{\alpha \tau}{P_0}\right) - \int_0^t dt_1 \frac{V(t_1)}{R_1}, \quad t \ge \tau. \end{aligned} \tag{4}$$

Thus, the circuit equation of Fig. 4 becomes

$$\begin{aligned} V(t) = \frac{Q(t)}{C} &= \frac{P_0 A}{C}\frac{t}{\tau}\left(1 - \frac{\alpha t}{P_0}\right) - \frac{1}{C}\int_0^t dt_1 \frac{V(t_1)}{R_1}, \quad 0 \le t \le \tau, \\ &= \frac{P_0 A}{C}\left(1 - \frac{\alpha \tau}{P_0}\right) - \frac{1}{C}\int_0^t dt_1 \frac{V(t_1)}{R_1}, \quad t \ge \tau, \end{aligned} \tag{5}$$

When the release time, CR_1, is much greater than τ, then, the third term of the right hand side of Eq. (5) is ignored. The voltage V is measured with a resistive voltage divider, as shown in Fig. 4. The voltage V_1 recorded on the oscilloscope has the value of V times the ratio of the resistance of the oscilloscope R_2 (50 Ω) to the load resistance R_1, or

$$V_1(t) = \frac{R_2}{R_1} V(t).$$

The current I is measured by using a current transformer CT.

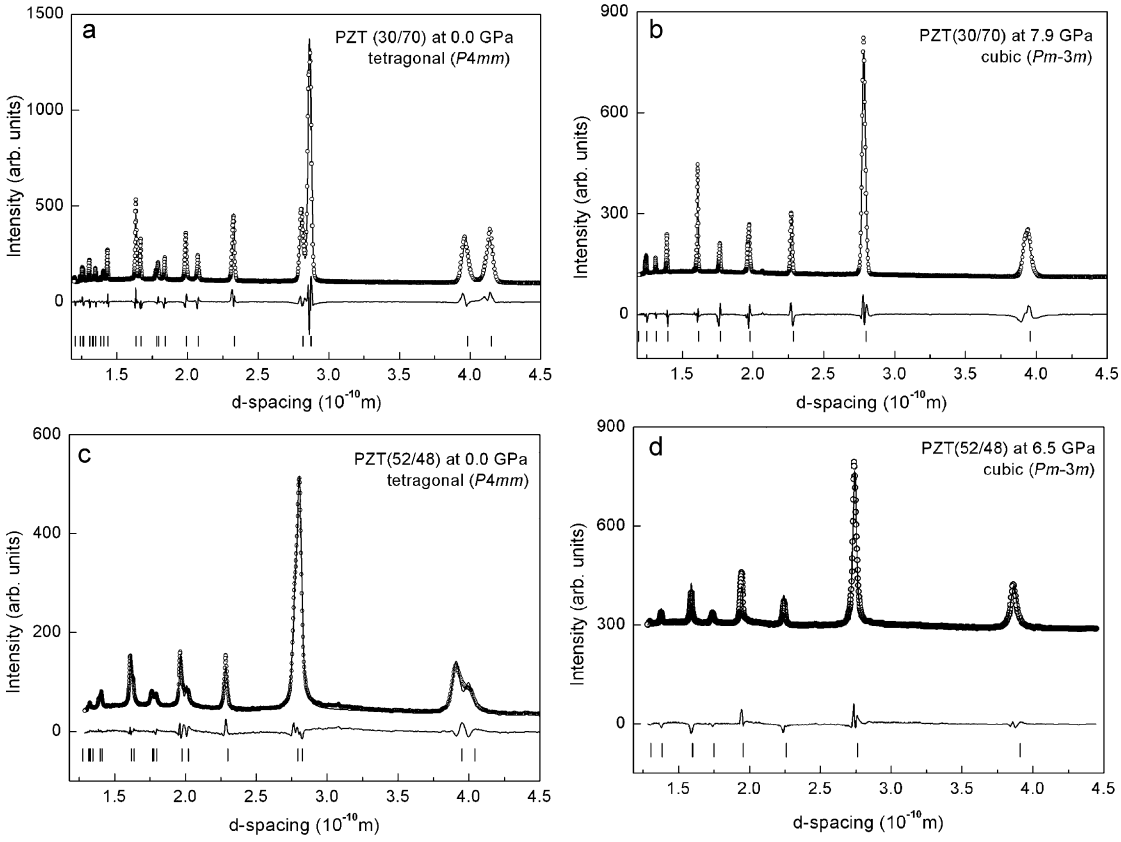

Fig. 5. The Rietveld refinement fit of the PZT(30/70) and PZT(52/48) ceramics. (The observed data are indicated by dots and the calculated pattern is the solid curve superimposed on them. The differences between the observed and calculated data are represented in the lower portion. Ticks are for PZT(30/70) and PZT(52/48) ceramics reflections.) (a) PZT(30/70) ceramic at 0 GPa. (b) PZT(30/70) ceramic at 7.9 GPa. (c) PZT(52/48) ceramic at 0 GPa. (d) PZT(52.48) ceramic at 6.5 GPa.

3. Results and discussion

3.1. High-pressure X-ray diffraction experiment

Upon compression to 30.1 GPa and 31.7 GPa for PZT(30/70) and PZT(52/48) ceramics respectively, a pressure-induced phase transition from tetragonal phase to cubic phase was observed for PZT(30/70) ceramic at ~7.4 GPa and PZT(52/48) ceramic at ~4 GPa. For PZT(30/70) and PZT(53/48) ceramics, Rietveld analyses[20,21] using a back ground, a zero-shift, a strain, a scale factor, cell constants, line shape parameters, isotropic atomic displacement parameters, atomic positions, and occupancies were performed on not only the powder patterns of PZT(30/70) ceramic at 0 GPa and 7.9 GPa but also the powder patterns of PZT(52/48) ceramic at 0 GPa and 6.5 GPa (Fig. 5).

To extract unit-cell volumes at high pressures that were used to draw a pressure–volume diagram at room temperature, Rietveld refinement using a back ground, a zero-shift with restraint, a strain, a scale factor, and cell constants was performed on not only the powder patterns obtained for PZT(30/70) ceramic at high pressures other than 0 GPa and 7.9 GPa but also those for PZT(52/48) ceramic at high pressures other than 0 GPa and 4.2 GPa. The space group *P4mm* (tetragonal phase) and $Pm\bar{3}m$ (cubic phase) were used for PZT(30/70) and PZT(52/48) ceramics at ambient pressure and transformed pressure, respectively.[22,23] A preferred orientation parameter was not used for PZT(30/70) and PZT(52/48) ceramics. The structure of PZT(30/70) ceramic is tetragonal in space group *P4mm* with lattice parameters $a = b = 3.9843 \pm 0.0003$ Å and $c = 4.1545 \pm 0.0003$ Å at 0 GPa. The high-pressure phase is cubic in space group $Pm\bar{3}m$ with lattice parameter $a = 3.9600 \pm 0.0003$ Å at 7.4 GPa. The structure of PZT(52/48) ceramic is tetragonal in space group *P4mm* with lattice parameters $a = b = 3.9508 \pm 0.0006$ Å and $c = 4.0414 \pm 0.0007$ Å at 0 GPa. The high-pressure phase is cubic in space group $Pm\bar{3}m$ with lattice parameter $a = 3.9186 \pm 0.0007$ Å at 4.2 GPa. Several structure parameters of PZT(30/70) and PZT(52/48) are given in Table 1.

In case of PZT(30/70) ceramic, a pressure-induced phase transition at ~7.4 GPa was observed (Fig. 6).[10] The B_0 of 83.9 ± 1.7 GPa for tetragonal phase and the B_0 of 102.5 ± 4.4 GPa for cubic phase were obtained where B_0' is fixed to 4.0. For PZT(52/48) ceramic, a pressure-induced phase transition at ~4 GPa was observed (Fig. 7). The B_0 of 49.6 ± 6.7 GPa for tetragonal phase and the B_0 of 87.5 ± 5.9 GPa for cubic phase were obtained where B'_0 is fixed to 4.0. The Birch-Murnaghan equation of state,[24,25] Eq. (6), derived from the data are plotted in Fig. 8.

$$\frac{P(f)}{3f(1+2f)^{5/2}} = B_0(1 + \alpha f + \beta f^2 + \ldots), \quad (6)$$

Table 1
Structural parameters of PZT(30/70) and PZT(52/48).

PZT material	Space group	Atomic position				B_{iso} (Å^2)		R_{wp}	R_{exp}	R_{Bragg}	GOF (χ^2)
			x	y	z						
30/70	$P4mm$	Pb	0	0	0	Pb	1.00 ± 0.08	6.67	8.54	3.57	0.78
		Zr/Ti	1/2	1/2	0.4449 ± 0.0029	Zr/Ti	0.10 ± 0.17				
		O1	1/2	1/2	0.1243 ± 0.0046	O1	0.97 ± 0.47				
		O2	1/2	0	0.6132 ± 0.0061	O2	0.97 ± 0.47				
30/70	$Pm\bar{3}m$	Pb	0	0	0	Pb	0.91 ± 0.10	1.27	3.69	1.70	0.35
		Zr/Ti	1/2	1/2	1/2	Zr/Ti	0.01 ± 0.20				
		O	1/2	1/2	0	O	0.99 ± 0.48				
52/48	$P4mm$	Pb	0	0	0	Pb	1.00 ± 0.08	6.45	12.67	3.02	0.51
		Zr/Ti	1/2	1/2	0.4715 ± 0.0043	Zr/Ti	0.85 ± 0.14				
		O1	1/2	1/2	0.2176 ± 0.0085	O1	0.00 ± 0.43				
		O2	1/2	0	0.4518 ± 0.0084	O2	0.00 ± 0.43				
2/48	$Pm\bar{3}m$	Pb	0	0	0	Pb	1.00 ± 0.13	2.17	6.18	2.24	0.35
		Zr/Ti	1/2	1/2	1/2	Zr/Ti	0.01 ± 0.20				
		O	1/2	1/2	0	O	0.01 ± 0.47				

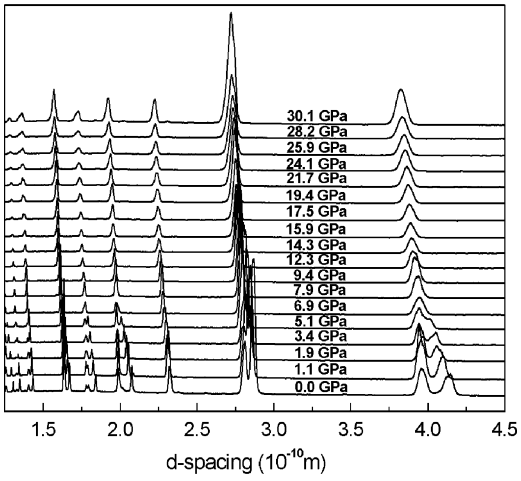

Fig. 6. X-ray diffraction spectra for PZT(30/70) ceramic at pressure up to 30.1 GPa. Notable changes are shown in spectra above 6.9 GPa, ascribed to the tetragonal – cubic transition.

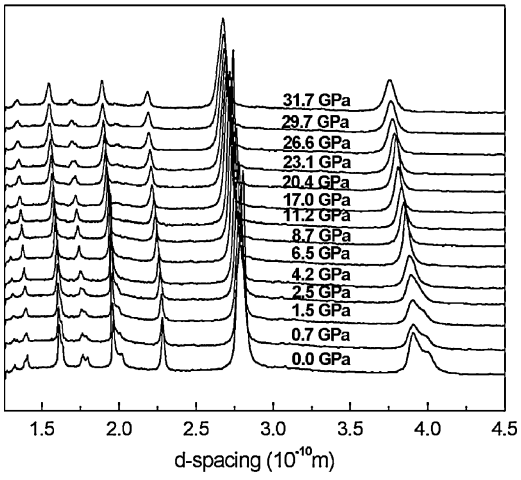

Fig. 7. X-ray diffraction spectra for PZT(52/48) ceramic at pressure up to 31.7 GPa. Notable changes are shown in spectra above 2.5 GPa, ascribed to the tetragonal – cubic transition.

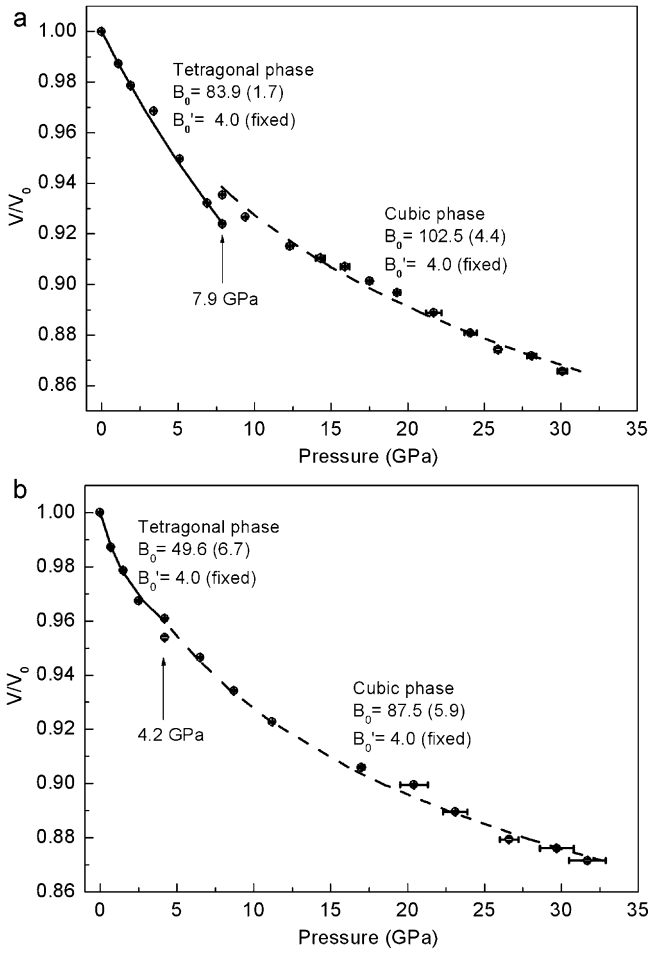

Fig. 8. Circles represent static compression data for PZT(30/70) and PZT(52/48) ceramics collected at 300 K and the curved line shows the Birch-Murnaghan equation of state fit to the data. (a) PZT(30/70) ceramic. (b) PZT(52/48) ceramic.

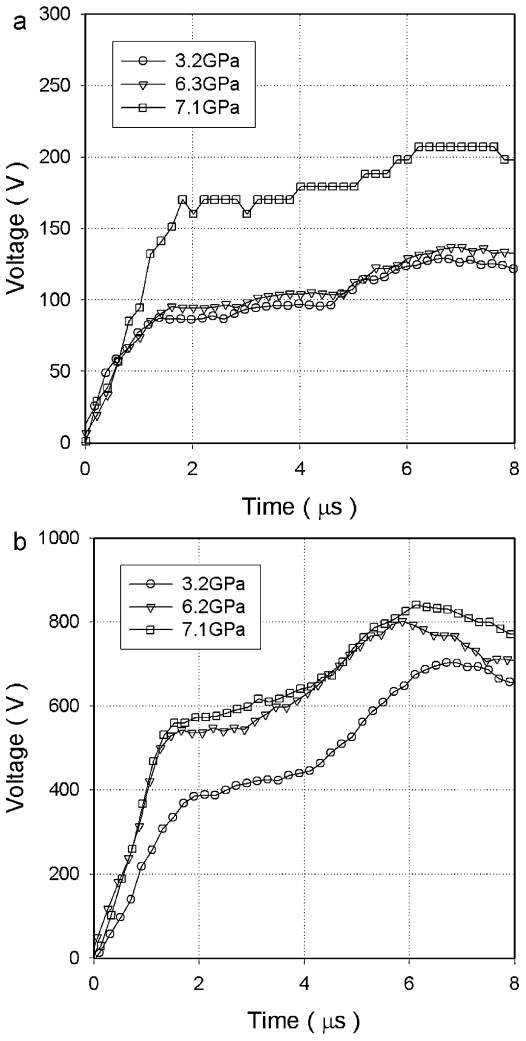

Fig. 9. Output voltage as a function of impact pressure (a) PZT(30/70) ceramic. (b) PZT(52/48) ceramic.

where f, α, and β are defined as

$$f = 0.5\left\{\left(\frac{V}{V_0}\right)^{-2/3} - 1\right\},$$

$$\alpha = 1.5(B'_0 - 4),$$

$$\beta = 1.5\left\{B_0 B''_0 + B'_0(B'_0 - 7) + \frac{143}{9}\right\},$$

with V_0 being unit cell volume at zero pressure, where B_0, B'_0, and B''_0 are defined as B_0: isothermal bulk modulus, $B'_0 = dB_0/dP$, $B''_0 = d^2B_0/d^2P$.

However, our results on transition to a cubic phase and no observation of deviation from cubic symmetry above ~4 GPa using synchrotron X-ray diffraction for PZT(52/48) ceramic are in very good agreement with Rouquette group's results that were measured using a laboratory source,[22] we could not observe low pressure or high pressure monoclinic phase between tetragonal and cubic phase.

3.2. Dynamic impact experiment

Fig. 9 is the result of measuring the output voltage of the PZT(30/70) and PZT(52/48) ceramics in the various impact pressure ranges by using the gas gun. The impact pressures were numerically calculated using hydrocode ANSYS AUTODYN.[26] In any experiment, the electrical breakdown was not observed and the waveforms of output voltages were similar. However, sudden increase of the output voltage at certain pressure was shown in both samples. The pressure of PZT(30/70) and PZT(52/48) ceramics was ~7 GPa and ~4 GPa respectively and each pressure was very similar to the pressure in which the phase transition occurs if the temperature increase of samples after shock loading, and the calculation error of impact pressure and the phase transition pressure were considered. The sudden increase of the output voltage may then be because complete depoling did not occur by domain switching below the phase transition pressure but complete depoling occurred by phase transition above phase transition pressure.

Many structural parameters such as elastic constants and piezoelectric constants change as a function of pressure, especially in the vicinity of the phase transition. Although the change of elastic constants and piezoelectric can affect impact induced output voltage, electric generation by shock wave is a very complex problem and we think that the effect of such parameters is trivial. In these experiments, electric generation was occurred by depoling, and piezoelectric charge generation could be ignored as written in introduction. Therefore the effect of piezoelectric constants on output voltage can be neglected. All the experimental pressures were higher than Hugoniot elastic limit of PZT(52/48),[27] presumed to be same in the case of PZT(30/70), so deformation by shock stress occurred plastically. Therefore effect of elastic constants on output voltage also can be ignored.

4. Conclusions

In this study, impact experiments of PZT(30/70) and PZT(52/48) ceramics were conducted by employing shock reverberation technique and X-ray diffraction patterns of these materials under high pressure. The tetragonal-to-cubic phase transition occurs at ~7.4 GPa for PZT(30/70) ceramic and at ~4 GPa for PZT(52/48) ceramic. The fit of the Birch-Murnaghan EOS to the data for PZT(30/70) ceramics gave $B_0 = 83.9 \pm 1.7$ GPa for tetragonal phase and $B_0 = 102.5 \pm 4.4$ GPa for cubic phase with $V_0 = 61.01 \pm 0.01$ Å^3 ($B'_0 = 4.0$) and those for PZT(52/48) ceramics gave $B_0 = 49.6 \pm 6.7$ GPa for tetragonal phase and $B_0 = 87.5 \pm 5.9$ GPa for cubic phase with $V_0 = 63.08 \pm 0.02$ Å^3 ($B'_0 = 4.0$). Electrical energy of PZT(30/70) and PZT(52/48) was generated by dynamic pressure using a 40-mm-bore gas gun for several shock pressure. As pressure increased, output voltage of PZT(30/70) and PZT(52/48) ceramics slightly increased below or above transition pressure, but the voltage significantly increased near transition pressure. Significant increase of output voltage near phase transition pressure was probably because complete depoling was occurred by phase transition.

References

1. Jaffe B, Cook WR, Jaffe H. *Piezoelectric ceramics*. London: Academic Press; 1971.
2. Heywang W, Thoman H. Tailoring of piezoelectric ceramics. *Annu Rev Mater Sci* 1984;**14**:27–47.
3. Scott JF, Araujo CA. Ferroelectric memories. *Science* 1989;**246**: 1400–5.
4. Xu Y. *Ferroelectric materials and their applications*. Amsterdam: North Holland; 1990.
5. Setter N, Colla EL. *Ferroelectric ceramics*. Boston: Birkhauser Veriag; 1993.
6. Kim HW, Priya S, Uchino K, Newnam RE. Piezoelectric energy harvesting under high pre-stresses cycle vibrations. *J Electroceram* 2005;**15**:27–34.
7. Keawboonchuay C, Engel TG. Design, modeling, and implementation of a 30 kW piezoelectric pulse generator. *IEEE Trans Plasma Sci* 2002;**30**:679–86.
8. Keawboonchuay C, Engel TG. Maximum power generation in piezoelectric pulse generator. *IEEE Trans Plasma Sci* 2003;**31**:123–8.
9. Linde RK. Depolarization of ferroelectrics at high strain rates. *J Appl Phys* 1967;**38**:4839–42.
10. Ko YH, Kim KJ, Cho KH, Seo CE. Crystal structure and compressibility of $Pb(Zr_{1-x}Ti_x)O_3$ ceramics under high pressure. *J Am Ceram Soc* 2010;**93**:1523–6.
11. Ko YH, Kim KJ, Cho KH, Seo CE. X-ray diffraction measurement and equation of state for piezoelectric $Pb(Zr_{1-x}Ti_x)O_3$ ($x = 0.1$–0.8) under static compression. *Curr Appl Phys* 2011;**11**:1024–30.
12. Piermarini CJ, Block S, Barnett JD. Hydrostatic limits in liquids and solids to 100 kbar. *J Appl Phys* 1973;**44**:5377–82.
13. Chervin JC, Canny B, Mancinelli M. Ruby-spheres as pressure gauge for optically transparent high pressure cells. *High Pressure Res* 2001;**21**:305–14.
14. Piermarini CJ, Block S, Barnett JD, Forman RA. Calibration of the pressure dependence of the R1 ruby fluorescence line to 195 kbar. *J Appl Phys* 1975;**46**:2774–80.
15. Syassen K. Ruby under pressure. *High Pressure Res* 2008;**28**:75–126.
16. Hammersley AP, Svensson SO, Thompson A, Grrafsma H, Kvick A, Moy JP. Calibration and correction of distortions in two-dimensional detector systems. *Rev Sci Instrum* 1995;**66**:2729–33.
17. Bruker AXS TOPAS V4.2. General profile and structure analysis software for powder diffraction data-user manual. Karlsruhe, Germany: Bruker AXS; 2009.
18. Frantti J. Note of the recent structural studies on lead zirconate titanate. *J Phys Chem B* 2008;**112**:6521–35.
19. Mock Jr W, Holt WH. *J Appl Phys* 1978;**49**:5846–54.
20. Young RA. *The Rietveld method: international union of crystallography monographs on crystallography*. Oxford University Press; 1993.
21. Giacovazzo C, Monaco HL, Artioli G, Viterbo D, Milanesio M, Ferraris G, et al. *Fundamentals of crystallography: international union of crystallography monographs on crystallography*. Oxford University Press; 2011.
22. Rouquette J, Haines J, Bornard V, Pintard M, Papet P, Astier R, et al. Transition to a cubic with symmetry-breaking disorder in $Pb(Zr_{0.52}Ti_{0.48})O_3$ at high pressure. *Phys Rev B* 2002;**65**, 214102-1-214102-4.
23. Burns G, Glazer AM. *Space groups for solid state scientists*. Academic Press; 1990 [chapter 8].
24. Birch F. Elasticity and constitution of earth's interior. *J Geophys Res* 1952;**57**:227–86.
25. Murnaghan FD. The compressibility of media under extreme pressure. *Proc Nat Acad Sci U S A* 1944;**30**:244–7.
26. AUTODYN User Manua Version 12.1. Canonsburg, PA, USA: ANSYS, Inc.; 2009.
27. Reynolds CE, Seay GE. Two-wave shock structures in the ferroelectric ceramics barium titanate and lead zirconate titanate. *J Appl Phys* 1962;**33**:2234–41.